Near-edge x-ray absorption fine structure and Raman characterization of amorphous and nanostructured carbon films

C. Lenardi, P. Piseri, V. Briois, C. E. Bottani, A. Li Bassi et al.

Citation: J. Appl. Phys. **85**, 7159 (1999); doi: 10.1063/1.370527
View online: http://dx.doi.org/10.1063/1.370527
View Table of Contents: http://jap.aip.org/resource/1/JAPIAU/v85/i10
Published by the American Institute of Physics.

Near-edge x-ray absorption fine structure and Raman characterization of amorphous and nanostructured carbon films

C. Lenardi[a)]
Commission of the European Union, Institute of Advanced Materials Joint Research Centre, I-21020 Ispra (Va), Italy

P. Piseri
INFM, Dipartimento di Fisica, Università di Milano, via Celoria 16, I-20133 Milano, Italy

V. Briois
LURE, Centre Universitaire Paris-Sud, Batiment 209D, I-91405 Orsay Cedex, France

C. E. Bottani and A. Li Bassi
INFM, Dipartimento di Ingegneria Nucleare, Politecnico di Milano, Via Ponzio 34/3, I-20133 Milano, Italy

P. Milani
INFM, Dipartimento di Fisica, Università di Milano, via Celoria 16, I-20133 Milano, Italy

(Received 17 September 1998; accepted for publication 29 January 1999)

Amorphous and nanostructured carbon films were grown by using two different techniques: ion sputtering and cluster beam deposition. The films were studied by near-edge x-ray absorption fine structure (NEXAFS) and Raman spectroscopy. Depending on the precursors, atoms, or clusters, the films are characterized by a different sp^2/sp^3 ratio which influences the mechanical and the electronic properties. Due to the sensitivities of NEXAFS (local order) and Raman (medium-range order), we have characterized and compared the structure of the films over different length scales. The complementarity of NEXAFS and Raman techniques for the characterization of disordered forms of carbon is here presented and discussed. We also present an original method of NEXAFS spectra calibration allowing a better determination of peak positions. © *1999 American Institute of Physics.* [S0021-8979(99)05309-8]

I. INTRODUCTION

Amorphous carbon films with a high content of sp^3 hybridized carbon have usually been associated with mechanical applications due to their high hardness, low friction coefficient, and chemical inertness.[1] More recently increasing interest in amorphous carbon films has arisen in view of their application in electronics and in particular as cathodes for field emission displays.[2] The capability of incorporating donors, like nitrogen, gives the further possibility of changing the optical band gap and consequently the electronic properties.[3]

Electronic and structural properties of carbon-based materials are strongly related to the different coordinations that carbon atoms can assume and to the dimensions and distributions of regions of homogeneous coordination in a sample. The tuning of the sp^2/sp^3 ratio is one of the most important requisites of all film deposition methods. As a result, advances have been made in the analytical techniques, enabling a quantitative determination of the sp^2/sp^3 ratio. However the knowledge of sp^2/sp^3 ratio alone is not enough to explain the characteristics of a material if this information is not corroborated by the distribution of sp^2 and sp^3 regions and their degree of order on length scales ranging from nm up to μm.[4]

Using physical vapor deposition (PVD), carbon films are synthesized atom-by-atom and the coordination is controlled by varying the kinetic energy of the deposited atoms.[3] Recently it has been proposed that the use of clusters instead of atoms as building blocks allows the synthesis of materials with novel structural and functional properties.[5,6] Nanostructured carbon thin films have been produced by depositing supersonic cluster beams.[5] Since the clusters retain their individuality, with low deposition energies, the physical and chemical properties of these materials are related to the local structure of the clusters as well as their size. It is then important to characterize the nanostructured material over different ranges of dimension in order to elucidate the local coordination of the cluster structure.

The subject of this work is the investigation of the structural and electronic properties of amorphous carbon films grown by ion sputtering and of nanostructured carbon films synthesized by cluster beam deposition (CBD). Two samples were also irradiated with 10 keV nitrogen ions in order to study the structural modifications of these materials. A few nanostructured samples were sputtered *in situ* both to remove surface contamination (in particular oxygen and hydrocarbon species) and to verify the surface modifications induced also by a light etching.

The determination of the coordination of the carbon atoms has been obtained principally by near-edge x-ray absorption fine structure spectroscopy (NEXAFS) while Raman spectroscopy has given complementary information on

a)Corresponding author; electronic mail: cristina.lenardi@jrc.it

the film structure.[7] Raman spectroscopy is sensitive to the structural changes in carbon-based materials, but if visible range photons are used, as in our case, a resonance effect in the cross section of sp^2 hybridized carbon takes place.[8] Thus no quantification of the sp^2/sp^3 ratio can be reliably performed. On the other hand, x-ray absorption at the carbon *K* edge depends principally on the atomic number *Z* and consequently the cross section is independent of the carbon atom coordination. The $1s \rightarrow \pi^*$ and $1s \rightarrow \sigma^*$ resonances in sp^2 carbon and $1s \rightarrow \sigma^*$ resonance in sp^3 carbon present a distinguishable difference in energy and a simple identification of each contribution can be made. Thus a quantitative determination of the amount of sp^2 can be performed. On the other hand the length scales typical of the Raman and NEXAFS are substantially different.

We will show that the combination of these two techniques can provide useful information on the structure of the different types of carbon films and help in elucidating differences originating from the use of different deposition methods. We will also show that for a correct interpretation of the experimental results, the sensitivity of NEXAFS and Raman over different length scales and to different carbon coordination must be taken into account. A method for NEXAFS spectra calibration is described in Sec. III A. The method allows a more precise determination of peak positions in the pre-edge region of the spectra.

II. EXPERIMENT

Amorphous carbon films were grown by sputtering a graphite target (purity$>$99.99 at. %) by argon ions using a Kaufman source of 3 cm diameter. The deposition apparatus has been described in detail in Ref. 9. The vacuum chamber was evacuated by a 450 $\mathrm{l\,s^{-1}}$ turbomolecular pump at the pressure of 3×10^{-7} mbar. The sputtering ion source was operated at voltages between 700 and 1000 V with a total beam current of 10–30 mA. At flow rates of 5 sccm for the sputter gun, the working gas pressure was $\leqslant 5\times10^{-4}$ mbar. The substrates were usually sapphire and silicon wafers (100 oriented). These were cleaned in a ultrasonic bath for 3 min, first with a cleaning solution, then with distilled water, and finally with propanol. Before the deposition the substrates were sputtered cleaned with a 500 V/10 mA nitrogen ion beam for 5 min. The substrates were glued to the sample holder by means a high thermal conductivity carbon glue. A few films were synthesized at room temperature. For another series of samples the substrate holder was cooled down to 80 K using liquid nitrogen and the substrate temperature monitored by a PT100 thermocouple. In this work the experimental results regarding the samples indicated as *S*#1(*a*-C) (sputtering voltage 1000 V, deposition at room temperature) and *S*#2(*a-C*) (sputtering voltage 700 V, deposition at 80 K) are presented.

Nanostructured carbon thin films were produced by deposition of carbon clusters in a supersonic beam.[5,6,10] The cluster beam apparatus has been described in detail elsewhere,[11] we report here only schematically the operation principles of the cluster source. Carbon is vaporized in a cavity inside the source body by an electrical discharge between two graphite electrodes. Cluster condensation is promoted by mixing the vapor with a pulse of an inert gas (He). The source geometry and operation principles have many similarities with a conventional Kraetschmer–Huffman (K–H) reactor for the production of fullerene soot,[12] nevertheless, the mechanism of carbon sputtering is substantially different. In our case, carbon atoms are vaporized from the cathode by intense plasma sputtering rather than by thermal effects related to arc discharges. The He-cluster mixture is expanded through a nozzle in a vacuum chamber under conditions suitable for the formation of a supersonic expansion. With standard operation conditions, the velocity of the carrier gas after the expansion is about 2000 m/s for aggregates in the front-end of the cluster beam pulse, while it is as low as 1000 m/s at the tail of the pulse (i.e., for the clusters which experience the longest residence time inside the source). The kinetic energy is thus lower than 0.25 eV/atom, i.e., well below the binding energy of carbon atoms in a cluster. In this kinetic energy regime the fragmentation of medium and large size carbon clusters (larger than several tens of atom per cluster) should be limited or even absent.

Mass spectrometric investigation of the cluster beam revealed a log–normal mass distribution peaked at 400 atoms per cluster, with a tail that extends towards higher masses up to about 1500 carbon atoms per cluster. Residence time inside the source is believed to be the main parameter controlling cluster size, as derived from mass spectra taken at different delay times after the discharge.[13] When depositing the aggregates upon a substrate, one has to take into account the fact that during each gas pulse the beam composition varies because of the different residence times experienced by the clusters in the front end of the pulse, compared to those in the tail. The effective composition of the beam is thus an average over all possible residence times, weighted by an instantaneous intensity. One possibility to adjust the mean residence time of the deposited beam is to vary the nozzle diameter and thus time necessary for emptying the source.

Two films were deposited, one with a 2 mm [sample *S*#3(CBD)] and the other with a 3 mm [sample *S*#4(CBD)] nozzle diameter. The clusters produced using the 2 mm nozzle have an average size 25% larger than those produced using the 3 mm nozzle.

After some hours of operation an anodic deposit (henceforth referred to as ''Anode'') grows inside the source. This deposit is rather similar to the cathodic one which grows in classical arc discharge reactors (K–H) for fullerene and nanotube production. Structural investigation performed by transmission electron microscopy (TEM) reveal a disordered graphitic material rich of nanotubes and multiwalled hollow particles (carbon onions). This result is also supported by Raman spectra and NEXAFS data presented in the present work.

Twin samples of *S*#1(*a*-C) and *S*#3(CBD) were ion implanted in a DANFYSIK 1090 high current implanter. A N^+ ion beam of 10 keV energy hits the samples with a dose of 10^{17} and 10^{16} ions/cm^2, respectively. In order to implant the ions as near as possible to the film surface we chose the lowest ion energy available from the implanter. The beam current density was maintained at 3.2 μA/cm^2 to reduce any

structural change induced by the temperature increase.

The density of the amorphous films was obtained from x-ray reflectivity using an in-house constructed glancing angle x-ray diffractometer. The film density was about 2.1 g/cm^3. Their elastic modulus E and the hardness H were measured by an ultralow depth sensing nanoindenter (Nano Instruments-Type II) from the loading-unloading curves. The displacement rate was maintained constant (3 nm/s) during the loading segment until the final depth of ~50 nm was reached. A peak-load segment was included for allowing the relaxation of the time-dependent plastic effects. The unloading segment was obtained by decreasing the loading force at a constant rate. The geometry and the stiffness of the tip were taken into account to provide accurate determination of E and H. The measured elastic modulus and hardness for the sample $S\#1(a\text{-C})$ were 250 and 25 GPa, respectively, and for the sample $S\#2(a\text{-C})$ were 220 and 20 GPa, respectively.

The mass density of the CBD films was evaluated by optical[5] and Brillouin[14] measurements performed on samples deposited in the same conditions of those presently investigated. The n and k values measured by optical ellipsometry had absolute values that were consistent, in the framework of Bruggeman effective-medium approximation,[15] with a porous structure containing a 0.5 fraction of voids.[5] On the other hand, elastic moduli, extracted from different peaks in Brillouin scattering spectra, fitted well together if a density of 1.1 g/cm^2 was assumed.[14] These evaluations have been confirmed by x-ray reflectivity measurements.[16] Bulk and surface Brillouin scattering measurements allowed the determination of the bulk modulus (3.7 GPa) and of the shear modulus (4 GPa).[17]

Mechanical properties of CBD samples were not determined by nanoindentation methods due to the high surface roughness related to the nanostructured nature of the films.

III. NEXAFS

A. Experiment and data handling

The NEXAFS experiments were carried out at LURE, France, on the vacuum ultraviolet (VUV) Super-ACO storage ring using the SACEMOR beamline. The monochromator was a high-energy toroidal grating monochromator (HE-TGM) with a rated energy resolution of 0.1 eV at the carbon K edge. The detection of electrons coming from the sample was performed in the total electron yield (TEY) mode. The energy step was 0.1 eV and the collecting time was 1 s for each channel. The intensity of the incident photon beam I_0 was measured from the photocurrent induced into an 85% transmission gold coated grid. The absorption signal was given by the ratio between the out-coming electron intensity from the sample I_s and the intensity I_0. For comparison, the spectra of a graphite sheet (purity 99.95%) and of diamond powder were collected. The diamond was also characterized by x-ray diffraction (XRD) in order to verify the good quality and to identify the eventual presence of other phases. A small quantity of non sp^3 bonds was also found in the C K-edge NEXAFS spectra. All the spectra were collected at a photon incidence angle of 55° (''magic angle'') to suppress the effects related to the x-ray polarization. The samples were exposed to air for a few months before being examined. At first we acquired spectra of all samples without them being subjected to any cleaning procedure, in order to avoid structural change of the phases contained in the films. Afterwards a few of the CBD samples were etched with a 600 eV/8 μA argon ion beam for 10 min in order to remove surface contamination and to induce surface modifications.

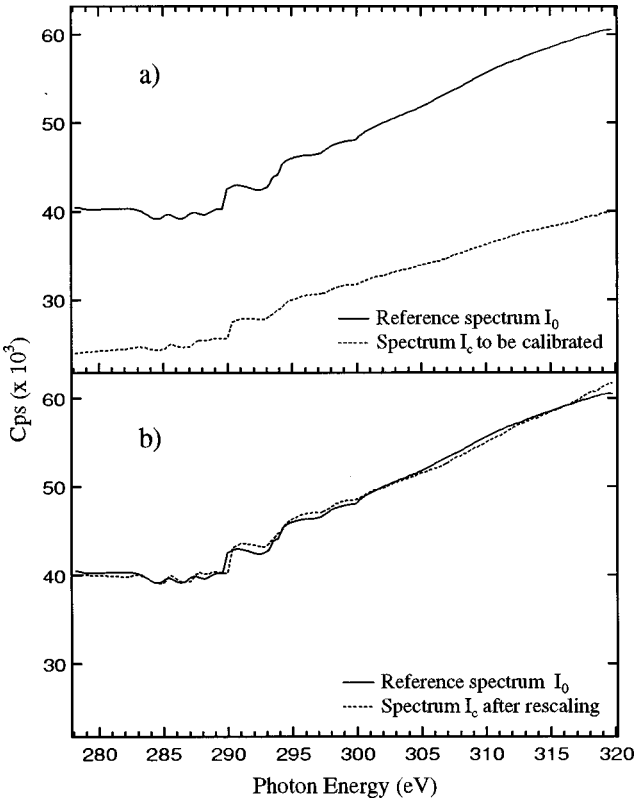

FIG. 1. The calibration procedure of the C 1s spectra by using the I_0 spectrum. (a) The reference I_0 spectrum (solid line) and a I_0^c spectrum to be calibrated (dashed line); (b) the reference I_0 spectrum (solid line) and the I_0^c spectrum after rescaling (dashed line).

Besides the C K-edge spectra we acquired NEXAFS data at O K edge and for the nitrogen implanted samples also at the N K edge.

Although the optical grade of the monocromator system could give an energy resolution of 100 meV, mechanical imprecision of the grating positioner leads to an energy shift between different spectra, with a standard deviation of nearly 0.5 eV. Thus we developed a calibration procedure based on the comparison of TEY spectra from the gold grid (I_0). The quantum efficiency of gold is rather smooth over the energy range of interest for carbon, nitrogen, and oxygen 1s near edge spectra; nevertheless, due to residual surface contamination of the beam optics and of the gold grid, some features are distinguishable over the smooth background and can be used for relative calibration of the spectra. Figure 1(a) shows two of these TEY spectra. The difference in intensity of the two spectra is due to slow variation of the x-ray beam flux and can be taken into account by multiplying one of the two spectra by a second order polynomial function of the energy. This is performed as the x-ray beam intensity can drift while

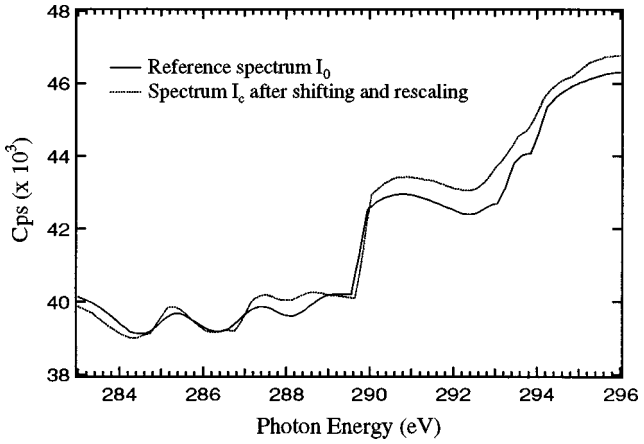

FIG. 2. A detailed section of the reference spectrum (solid line) and of the spectrum I_0^c after rescaling and shifting (dashed line).

the energy is slowly scanned over the spectral range of interest, and corrections up to a second order in time (i.e., in energy) must be taken into account if one wants to compare features appearing in different spectra. Figure 1(b) shows the same spectra as Fig. 1(a) after the rescaling procedure described above. The polynomial coefficients are chosen in order to obtain the best fit. Figure 2 shows a detail of two spectra after shifting of one spectrum with respect to the other. For each spectrum we tried different shifts, fitting again the polynomial coefficients each time. The shift giving the minimum difference between the spectra has been used to correct the energy scale of the given spectrum. The shifts of all the spectra with respect to the reference one follow a Gaussian distribution that is not centered upon zero because the reference spectrum is randomly chosen. As the monochromator is supposed to be calibrated, we believe that the spectra falling at the mean of the Gaussian have the best absolute energy calibration among all the measurements we have acquired. Thus we have subtracted the mean position from the energies of all the acquired spectra. Many spectra do not perfectly fit to the reference spectrum if rigidly shifted; this suggests that distortion of the energy scale should be introduced to perform a better relative calibration of the spectra. For the purpose of this work we believe it is not worth refining further the energy scale correction. In fact, NEXAFS spectra of disordered structures show only broad features whose identification ambiguity would not be removed by a more accurate energy calibration. Nevertheless, the method used has given direct evidence that an energy shift of the $1s \rightarrow \pi^*_{C=C}$ transition is correlated to distortion of the sp^2 hybridization.

B. Results

The NEXAFS C *K*-edge spectra of as-deposited amorphous (*a*-C) and nanostructured (CBD) films are shown in Fig. 3. For comparison the spectra of graphite and diamond are also reported in the figure together with the spectrum of the deposit on the anode in the cluster beam source (sample Anode), which will be used as reference for the evaluation of the sp^2 content in the carbon films as extensively described later on. Figure 4 shows the C *K*-edge spectra of an amorphous and a nanostructured film as-deposited and after nitrogen implantation. Finally the C *K*-edge spectra of nanostructured films before and after the *in situ* etching are reported in Fig. 5.

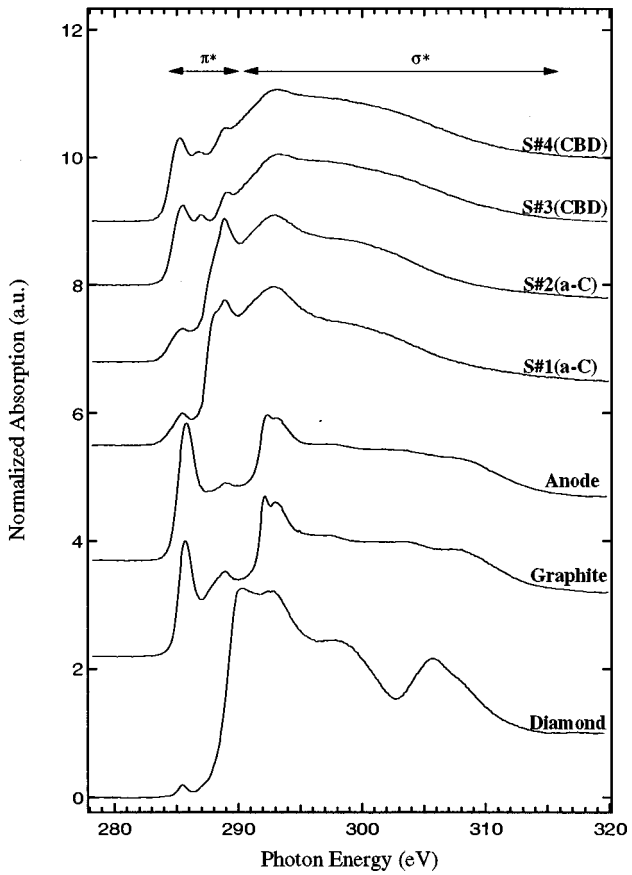

FIG. 3. The NEXAFS C *K*-edge spectra of as-deposited amorphous and nanostructured carbon films. The anodic deposit grown in the cluster source is indicated as Anode. It has been used as 100% sp^2 reference sample for the evaluation of the sp^2 content of the carbon films. For comparison the spectra of graphite and diamond powder are also shown.

The shape of the graphite spectrum is similar to that of graphite spectra reported in the literature.[18] The diamond spectrum shows the characteristic feature at 302.7 eV related to the second absolute gap.[19] Nevertheless the sharp core exciton peak[20] at about 0.2 eV below the onset of $1s \rightarrow \sigma^*$ transitions ($\simeq$288.5 eV) cannot be resolved.

In Figs. 3–5 the spectra of *a*-C and CBD samples show a pre-edge resonance at about 285.3 eV due to transitions from the C 1*s* level to unoccupied π^* states of sp^2 (C=C) sites, with eventually also the contribution of *sp* (C≡C) sites if present. This peak is also present in the diamond spectrum and originates from a graphitic phase contained in the material already detected by x-ray diffraction measurements. Another relevant peak arises at $\simeq$288.8 eV, more evident in the amorphous carbon films and reduced after etching in the CBD samples. The as-deposited CBD samples show also a prominent resonance at $\sim$286.8 eV partially reduced after etching and implantation. The amorphous nature of the films induces a spread of the σ^* resonances and no recognizable structures can be identified. Thus the broad band be-

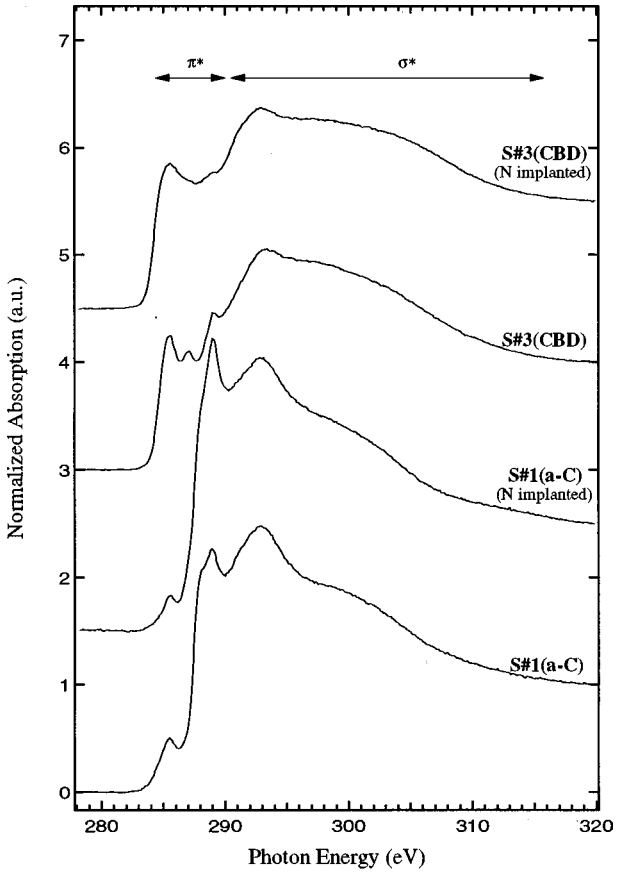

FIG. 4. The NEXAFS C *K*-edge spectra of the implanted samples *S*#1(*a*-C) and *S*#3(CBD) as deposited and after the implantation of a 10 keV N^+ ion beam with a dose of 10^{17} and 10^{16} ions/cm^2, respectively.

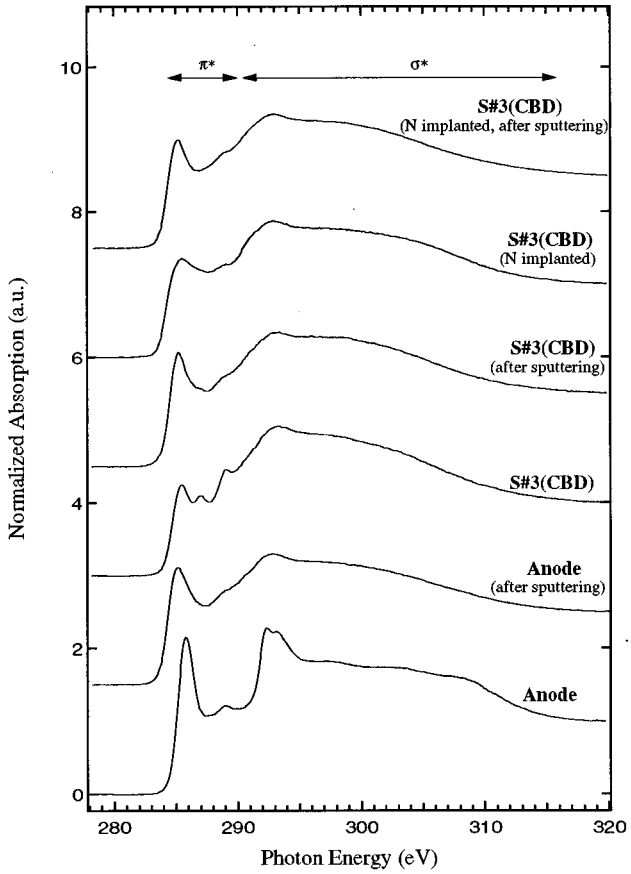

FIG. 5. The NEXAFS C *K*-edge spectra of the sputtered sample *S*#3(CBD) (as-deposited and after the nitrogen implantation) and of the Anode. The samples have been etched with a 600 eV/8 μA argon ion beam for 10 min.

tween 290 and 310 eV is the result of overlapping C 1*s* $\rightarrow\sigma^*$ transitions at *sp*, sp^2, and sp^3 sites.

The NEXAFS N *K*-edge spectra for the nitrogen implanted samples (containing approximately 20 at. % N in the implanted region), namely *S*#1(*a*-C) and *S*#3(CBD), have a very low intensity compared to N *K*-edge spectra of carbon nitride films containing a similar amount of N.[21] This confirms that the nitrogen ions penetrate more deeply than the region (100 Å in TEY mode) detected by NEXAFS, as expected by a simulation of the ion implantation process performed using the program PROFILE.[22] Due to the negligible presence of nitrogen, minimal contributions of C 1*s* transitions from carbon atoms bonded to nitrogen are expected in the C *K*-edge spectra.

The evaluation of the sp^2 content in the different samples requires the determination of the peak area of the $1s\rightarrow\pi^*_{C=C}$ resonance, as demanded by the procedure successively described. Thus, in order to also have a better insight in the spectral structure and to make an assignment of the identified resonances, we have peak fitted of the acquired spectra. The peak assignment and area evaluation is quite ambiguous in NEXAFS spectra of amorphous carbon, due to the broadening of the peaks themselves and to the overlapping contribution of wide and structured continuum steps. For this reason the attribution for the located peaks has been restricted only to the pre-edge region (roughly below 290 eV), and quantitative analysis has been limited to the the $1s\rightarrow\pi^*_{C=C}$ resonance.

To determine the position of the peaks in the pre-edge region, we have calculated the second derivative of the spectrum (c. c. Jaouen *et al.*).[19] Four principal minima have been found and the corresponding energies have been used as the initial inputs of the peak positions in the fit procedure. The pre-edge resonances have been fitted with symmetrical Gaussian curves. The width of these peaks is dominated by the disordered nature of the deposit. We have fitted only the width of the first peak while for the three others we have fixed the value at 1.2 eV.[19] The edge jump at the ionization potential has been represented by an erf function multiplied by an exponential decay. Since various shifts of the C 1*s* due to different chemical states are present, the use of only one step edge could be regarded as too rough an approximation. For this reason, we have considered the step width as a free parameter in the fit in order to include many different ionization potentials within a single broad step. For the best fit, a step width of about 0.9 eV is obtained. The σ^* resonance region has been fitted with two Gaussian curves having an exponential tail at higher energies and dropping down in a similar fashion to the step function at the absorption edge. An example of the fit for the nanostructured carbon film *S*#4(CBD) is given in Fig. 6.

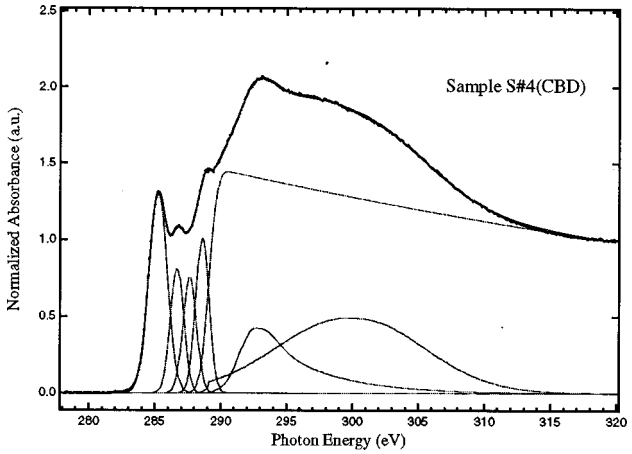

FIG. 6. Fit of the sample *S*#4(CBD). The solid line is the resulting fitted curve and the dotted lines are the individual components of the deconvolution.

The first peak (at 285.3 eV) is due to π^* antibonding orbitals principally originating from C═C bonds. The amount of this bond type can be partially overestimated in the case of CBD films since in these layers a certain proportion of C≡C bonds seem to be present (usually disregarded in amorphous films) and may therefore contribute to the area of $1s \rightarrow \pi^*$ resonance of C═C bond. The presence of *sp* hybridized carbons is suggested by a feature at $\sim 2150\ \mathrm{cm}^{-1}$ in the Raman spectra (not shown). Further investigation must be carried out to unambiguously attribute this feature to triple bonds and to eventually quantify the *sp* fraction.

The averaged full-width at half-maximum (FWHM) of the peak at 285.3 eV for the as-deposited *a*-C films is ~1.9 eV and for the as-deposited CBD films is ~1.7 eV. After the N implantation and/or sputtering the value is ~1.9 eV. For the graphite the FWHM is evaluated to be 1.1 eV and for the anode 1.3 eV. The width of the $1s \rightarrow \pi^*$ resonance of C═C bond is thus considered as an index of disorder on a local scale. This effect is correlated with the presence of different distorted sp^2 sites and defects. Furthermore the peak position lies at lower energy (a shift of ~0.4 eV) with respect to the graphite and the Anode for both types of prepared samples; from the energy calibration procedure we can exclude that this is due to some instrumental effect. Further investigation should be performed to determine to what extent this shift is correlated to bond distortion and whether it can be used as a reliable index for the determination of local structure.

The second peak (at 286.8 eV) is related to permitted transitions $1s \rightarrow \pi^*$ induced by the presence of oxygen. In the *a*-C samples this peak shows a significantly smaller intensity with respect to those of the nanostructured samples. For the amorphous films the origin of the peak lies principally in the oxygen at the surface. In fact photoelectron spectroscopy performed on the twin etched samples show negligible presence of oxygen inside the film. On the contrary in the CBD samples the intensity of the $\pi^*_{C=O}$ peak is only slightly reduced by the sputtering and this indicates that the oxygen is also present inside the sample. However the major effect of 600 eV/8 μA Ar^+ etching is the growth of the $\pi^*_{C=C}$ peak which masks the $1s \rightarrow \pi^*_{C=O}$ resonance.

The third peak at 287.8 eV is assigned to the $1s \rightarrow \sigma^*_{C-H}$ transition.[23] This peak is due to the contribution both to the hydrogen saturation of surface carbon dangling bonds and, to a smaller extent, the incorporation of hydrocarbon species in the films during the growing process. The resonance is correlated to the presence of sp^3 sites and in fact is higher in the case of *a*-C samples where the sp^2 content is smaller with respect to CBD samples. The peak is reduced after sputtering, but not completely removed. Instead, in the case of implantation the peak is strongly reduced showing the capability of highly energetic ions to break C–H bonds.

The last peak located in the pre-edge region is found at 288.8 eV. Jaouen *et al.*[19] assign this peak to $1s \rightarrow \pi^*$ transitions due to O═C–OH species. This assignment finds its principal justification in the shape of the O *K* edge which shows the $1s \rightarrow \pi^*_{O=C}$ transitions to be related to the presence of an alcohol functional group. Thus the reduced sp^2 fraction in the film is interpreted as an increment of hydrogen or O═C–OH acidic functional group as peripheral termination of the graphitic domains.

This assignment of Jaouen *et al.* cannot explain a few features present in our spectra: (i) this resonance is larger in the case of films with minor sp^2 content (*a*-C) but also having the lower content of oxygen. For *a*-C samples the height of the peak is comparable to the σ^* edge, while for the CBD ones the resonance appears as a shoulder on the onset of the σ^* edge. (ii) Sputtering as well as ion implantation do not considerably affect the peak shape and height with the exception of the Anode sample. In this case the peak increases while the $1s \rightarrow \pi^*_{C=C}$ resonance diminishes in height and increases in width, showing the known effect of Ar^+ sputtering on graphite: amorphization of the sample surface and promotion of sp^3 bond formation.[24] (iii) In the O *K*-edge spectra the etched and implanted samples show a strong reduction of the $1s \rightarrow \pi^*_{O=C}$ transition which completely disappears in the sputtered Anode spectrum. To explain these observations we consider that there should be a correlation between the presence of sp^3 sites and the resonance at 288.8 eV. Gutiérrez *et al.*[25] suggest that the peak can originate from an excitonic process in amorphous samples having sp^3 hybridized carbon atoms. The peak presents a shift, in our case of about 0.7 eV, with respect to the diamond exciton. Again Gutiérrez *et al.* indicate that this effect could be due to either a shift in a band edge position of amorphous carbon materials or in a change in the excitonic binding energy. This interpretation seems to give a more convincing explanation of our experimental results, and further experimental and theoretical work should be carried out on the topic.

In the limit of small momentum transfer, the electron energy loss spectroscopy (EELS) spectra are dominated by dipole transitions as in the case of the x-ray absorption spectra (for excitation of shells at wavelength ≫of the shell diameter).[23] Thus the well established method for determination of the sp^2 fraction from EELS[26,27] can be also applied to the NEXAFS measurements. The amount of sp^2 bonded carbon atoms can be extracted by normalizing

TABLE I. The sp^2 fraction as evaluated following the method described by Fallon.[a] All the results are referred to the sample Anode which is assumed to have 100% of sp^2 sites.

Sample	sp^2 content %
Anode	100.00
Anode (after sputtering)	89.32
S#1(*a*-C)	26.62
S#1(*a*-C) (N implanted)	14.32
S#2(*a*-C)	31.14
S#3(CBD)	62.87
S#3(CBD) (after sputtering)	81.95
S#3(CBD) (N implanted)	81.94
S#3(CBD) (N implanted, after sputtering)	82.86
S#4(CBD)	63.38

[a]See Ref. 27.

the area of the resonance corresponding to $1s \rightarrow \pi^*_{C=C}$ transition at 285.3 eV with the area of a large section of the spectrum and comparing this ratio with the value of the ratio obtained in the same way for a carbon film which contains a known fraction of sp^2 sites. In the case of a 100% sp^2 reference sample, the calculation is made by using the following expression

$$f_{sp^2} = \frac{I^{\pi^*}_{\text{sam}}}{I^{\pi^*}_{\text{ref}}} \frac{I_{\text{ref}}(\Delta E)}{I_{\text{sam}}(\Delta E)},$$

where $I^{\pi^*}_{\text{sam}}$ and $I^{\pi^*}_{\text{ref}}$ are the areas of the π^* peak of the carbon sample and the 100% sp^2 reference material, respectively, and $I_{\text{sam}}(\Delta E)$ and $I_{\text{ref}}(\Delta E)$ are the areas evaluated over the energy interval ΔE of the carbon sample and the reference material, respectively.

Since the intensity of the π^* peak of graphite depends on the angle of the impinging x-ray beam and other experimental parameters,[26] we have chosen the sample indicated as Anode in Fig. 3 as a reference. The highly disordered orientation of graphitic crystallites in this sample makes it more suitable than graphite as a reference for evaluation of sp^2 content in amorphous carbon. Its NEXAFS spectrum very closely resembles that of graphite and as a consequence we have assumed this sample to be a 100% sp^2 reference. The determined contents of sp^2 are reported in Table I.

IV. RAMAN

A. Experiment

Unpolarized Raman and micro-Raman spectra were recorded *ex situ*, at room temperature and in back scattering geometry. An I.S.A. Jobin–Yvon triple grating spectrometer and a liquid nitrogen cooled detector were used. The excitation source was the 514.5 nm line of an Ar ion laser; the estimated spectral resolution was about 3 cm^{-1}. The micro-Raman spectra were measured using a 100× objective. Power on the sample was monitored and always kept below 1 mW in the micro-Raman configuration to avoid sample degradation; this was checked by monitoring the changes in the graphitic features of the Raman spectra while increasing the laser power on the samples. No degradation was observed in the macro configuration, where 5–10 mW on the sample were used. No appreciable differences were seen between Raman and micro-Raman spectra.

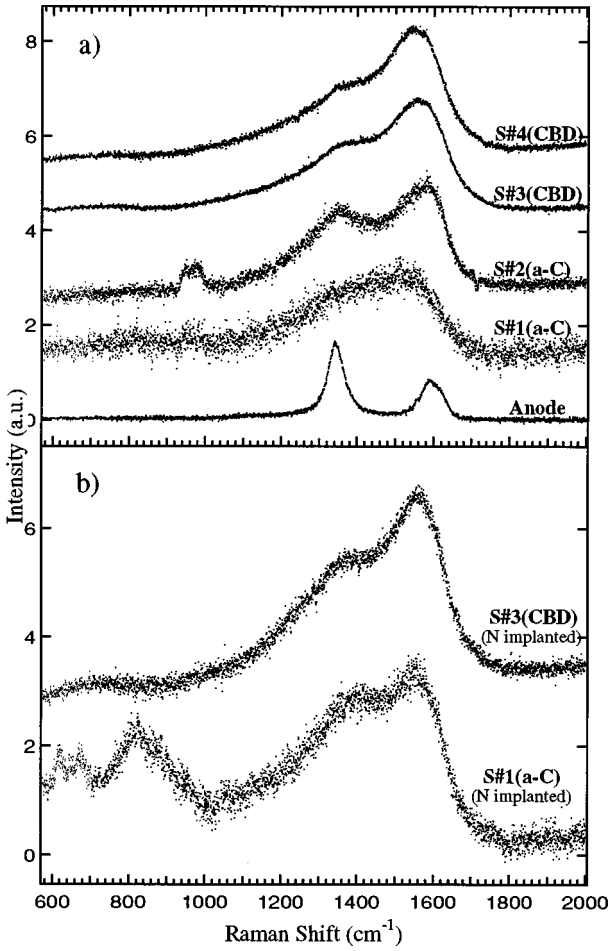

FIG. 7. Raman spectra of amorphous and nanostructured samples: (a) as deposited; (b) implanted. Due to the high optical transparency of the amorphous samples, the contribution of the silicon substrate is also detected by the peaks at ~1000 cm^{-1} (second order).

B. Results and Discussion

In Fig. 7 we report the Raman spectra of amorphous and nanostructured carbon films as deposited [Fig. 7(a)] and implanted [Fig. 7(b)]. In the frequency range below 1000 cm^{-1} we observe a broad hump extending from roughly 650 up to 800 cm^{-1} in the CBD samples;[28] this broad peak has been reported by Bacsa *et al.* for *a*-C and related to a peak in the phonon density of states (PDOS) of graphite.[29] The region between 1000 and 2000 cm^{-1} is characterized by a peak at about 1550–1600 cm^{-1} (the *G* band of the crystalline graphite arising from the zone-center E_{2g} phonon), with a shoulder at about 1350 cm^{-1} (due to the so-called *D* band, assigned to an A_{1g} zone-edge mode activated because of the finite size of the graphitic domains).[30–33]

In general, for all the as-deposited samples the recorded spectra are typical of a disordered carbon with a high degree of sp^2 carbon coordination. The spectral features relative to broadened and highly overlapping *G* and *D* bands suggest that the PDOS is different from that of graphite because of

the presence of various kinds of disorder (bond angle and length defects, different coordinations with respect to graphitic sp^2).[32] At this degree of disorder the Tuinstra–Koenig relationship[30,31,33,34] is not valid anymore. At a qualitative analysis level the spectra of nanostructured carbon films are basically independent of the deposition parameters and are not modified by N implantation. However, the films grown by ion sputtering have different degrees of order, in particular sample *S*#1(*a*-C) shows a more pronounced amorphous character which is reduced by N implantation.

To compare different samples on a more quantitative basis, we have fitted the spectra with a Lorentzian for the *D* peak and a Breit–Wigner–Fano (BWF) for the *G* peak,[35–37] since the asymmetry of the BWF takes into account the intensity due to the PDOS. The fitting shows that the *G* peak position in the amorphous films is in the range of 1540–1580 cm^{-1} (1570 cm^{-1} for sample *S*#1(*a*-C) N implanted), the *D* peak in the range of 1340–1380 cm^{-1}. The FWHM is in the range of 180–260 cm^{-1} for the *G* peak (230 cm^{-1} for *S*#1(*a*-C) N implanted) and in the range of 220–330 cm^{-1} for the *D* peak (260 cm^{-1} for *S*#1(*a*-C) N implanted). For all the nanostructured samples the *G* peak is located at about 1565 cm^{-1}, the *D* peak at about 1360 cm^{-1}. The FWHM of the *G* peak is 180 cm^{-1}, while it is in the range of 320–360 cm^{-1} for the *D* peak. Considering the correlation between BWF width and position as a reliable graphitization index for highly disordered carbons,[36] previous results show that the nanostructured films and sample *S*#2(*a*-C) have a comparable degree of order. In the case of the most amorphous film *S*#1(*a*-C), implantation at a dose of 10^{17} ions/cm^2 seems to cause an emergence of more distinct *D* and *G* bands suggesting that at this dose an increase in the order of sp^2 bonded structures within the implanted layer has occurred.[38]

V. CONCLUSIONS

Amorphous and nanostructured carbon films have different structures due to the different precursors (namely atoms and clusters) used for their deposition. These differences are reflected in the different mechanical behavior displayed by the two sets of samples. The samples grown by sputtering show a higher density and hardness compared to the CBD films. This is due to a different coordination (principally sp^3) and probably also to a different organization of the sp^3 regions in the amorphous films.

The average sp^2 content of the samples deposited by sputtering is ~29% while for nanostructured samples is ~63% for the as-deposited films and ~82% for the etched films. For the implanted sample *S*#3(CBD) the sp^2 content grows up to 82% that is the same amount obtained after etching of the as-deposited films. The sputtering of the sample does not modify further the sp^2 content in the film. Such effects are not clearly exhibited by the Raman spectra.

For the film *S*#1(*a*-C) the sp^2 content decreases from 27% down to 14% after implantation. On the contrary the Raman spectrum exhibits a qualitative change from a more disordered material to one having an increased medium-range order. This apparently contradictory response of the two techniques may be due to the different surface sensitiveness of the two techniques. In fact Raman is not sensitive to surface modifications while NEXAFS has a depth sensitivity of about 100 Å in the energetic range under investigation. Moreover Raman and NEXAFS probe different length scales and their varying sensitivity to different carbon coordinations should be also taken into account. Raman spectroscopy is sensitive on larger scale compared to NEXAFS and probes the degree of order over this scale, whereas NEXAFS is a more local probe insensitive to the relative organization of different coordination sites over more than a few tenths of a nanometer.

The fact that the large differences between the NEXAFS spectra of the two sets of samples are not reflected in the Raman spectra confirms that the two techniques probes different length scales and have different bond-type sensitivity. From the Raman spectra we can conclude that the samples are disordered on the scale of several nm and present a similar medium-range order, but they have different local coordinations as revealed by NEXAFS data. A comparison of the results from the two techniques confirms also that the determination of the sp^3 contents of carbon containing samples with Raman spectroscopy is very questionable if one uses a visible laser as an excitation source.[8]

We have shown that refined calibration of NEXAFS spectra may allow one to extract more precise information on local structure if energy shifts of the $1s \rightarrow \pi^*$ resonances are taken into account. The present results suggest that further investigation should be made on this subject.

ACKNOWLEDGMENTS

We acknowledge partial financial support from INFM under Advanced Research Project CLASS. The authors wish also to thank C. Laffon and Ph. Parent for their technical support at the SACEMOR beamline, R. Pastorelli for the Raman measurements, and H. Willers for the ion implantation.

[1] J. Robertson, Surf. Coat. Technol. **50**, 185 (1992).
[2] B. S. Satyanarayana, A. Hart, W. I. Milne, and J. Robertson, Appl. Phys. Lett. **71**, 1430 (1997).
[3] V. S. Veerasamy, J. Yuan, G. A. J. Amaratunga, W. I. Milne, K. W. R. Gilkes, M. Weiler, and L. M. Brown, Phys. Rev. B **48**, 17954 (1993).
[4] M. A. Tamor and C. H. Wu, J. Appl. Phys. **67**, 1007 (1990).
[5] P. Milani, M. Ferretti, P. Piseri, C. E. Bottani, A. Ferrari, A. Li Bassi, G. Guizzetti, and M. Patrini, J. Appl. Phys. **82**, 5793 (1997).
[6] P. Melinon, V. Paillard, V. Dupuis, A. Perez, P. Jensen, A. Hoareau, J. P. Perez, J. Tuaillon, M. Broyer, J. L. Vialle, M. Pellarin, B. Baguenard, and J. Lerme, Int. J. Mod. Phys. B **9**, 339 (1995).
[7] K. Edamatsu, Y. Takata, T. Yokoyama, K. Seki, M. Tohnan, T. Okada, and T. Ohta, Jpn. J. Appl. Phys., Part 1 **30**, 1073 (1991).
[8] K. W. R. Gilkes, H. S. Sands, D. N. Batchelder, J. Robertson, and W. I. Milne, Appl. Phys. Lett. **70**, 1980 (1997).
[9] P. Hammer and W. Gissler, Diamond Relat. Mater. **5**, 1152 (1996).
[10] E. Barborini, P. Piseri, A. Li Bassi, A. C. Ferrari, C. E. Bottani, and P. Milani, Chem. Phys. Lett. **300**, 633 (1999).
[11] P. Piseri, A. Li Bassi, and P. Milani, Rev. Sci. Instrum. **69**, 1647 (1998).
[12] P. Milani, Riv. Nuovo Cimento **19**, 1 (1996).
[13] A. Li Bassi, Degree thesis, Politecnico di Milano, 1997.
[14] C. E. Bottani, A. C. Ferrari, A. Li Bassi, P. Milani, M. Ferretti, and P. Piseri, Carbon **36**, 535 (1998).
[15] D. A. G. Bruggeman, Ann. Phys. (Leipzig) **24**, 636 (1935).
[16] A. Li Bassi and B. Tanner (unpublished).
[17] C. E. Bottani, A. C. Ferrari, A. Li Bassi, P. Milani, and P. Piseri, Europhys. Lett. **48**, 431 (1998).

[18] P. E. Batson, Phys. Rev. B **48**, 2608 (1993).
[19] M. Jaouen, G. Tourillon, J. Delafond, N. Junqua, and G. Hug, Diamond Relat. Mater. **4**, 200 (1995).
[20] J. F. Morar, F. J. Himpsel, G. Hollinger, G. Hughes, and J. L. Jordan, Phys. Rev. Lett. **54**, 1960 (1985).
[21] C. Lenardi, P. Piseri, and V. Briois (unpublished).
[22] PROFILE CODE, Vers. 3.18, Implant Science Corporation, Massachusetts (1991).
[23] J. Stöhr, *NEXAFS Spectroscopy* (Springer, New York, 1992).
[24] F. Atamny, J. Blöcker, B. Henschke, R. Schlögl, Th. Schedel-Niedrig, M. Keil, and A. M. Bradshaw, J. Phys. Chem. **96**, 4522 (1992).
[25] A. Gutiérrez, J. Díaz, and M. F. López, Appl. Phys. A: Solids Surf. **61**, 111 (1995).
[26] S. D. Berger, D. R. Mc Kenzie, and P. J. Martin, Philos. Mag. Lett. **57**, 285 (1988).
[27] P. J. Fallon, V. S. Veerasamy, C. A. Davis, J. Robertson, G. A. J. Amaratunga, W. J. Milne, and J. Koskinen, Phys. Rev. B **48**, 4777 (1993).
[28] F. Li and J. S. Lannin, Appl. Phys. Lett. **61**, 2116 (1992).
[29] W. S. Bacsa, J. S. Lannin, D. L. Pappas, and J. J. Cuomo, Phys. Rev. B **47**, 10931 (1993).
[30] F. Tuinstra and J. L. Koenig, J. Chem. Phys. **53**, 1126 (1970).
[31] D. S. Knight and W. B. White, J. Mater. Res. **4**, 385 (1989).
[32] R. J. Nemanich and S. A. Solin, Phys. Rev. B **20**, 392 (1979).
[33] R. O. Dillon, J. A. Woollam, and V. Katkanant, Phys. Rev. B **29**, 3482 (1984).
[34] J. Schwan, S. Ulrich, V. Batori, H. Ehrhardt, and S. R. P. Silva, J. Appl. Phys. **80**, 440 (1996).
[35] B. S. Elman, M. Shayegan, M. S. Dresselhaus, H. Mazurek, and G. Dresselhaus, Phys. Rev. B **25**, 4142 (1982).
[36] D. G. McCulloch, S. Prawer, and H. Hoffman, Phys. Rev. B **50**, 5905 (1994).
[37] D. G. McCulloch and S. Prawer, J. Appl. Phys. **78**, 3040 (1995).
[38] D. G. McCulloch, D. R. McKenzie, and S. Prawer, Philos. Mag. A **72**, 1031 (1995).